

COMPARISON OF CARBON AND METAL OXIDE ANODE MATERIALS FOR RECHARGEABLE LI-ION CELLS

C.-K. Huang¹, J. S. Sakamoto², M. C. Smart¹, S. Surampudi¹, and J. Wolfenstine²

¹Jet Propulsion Lab., California Institute of Technology, 4800 Oak Grove Drive, Pasadena, CA 91109

²University of California, Irvine, Dept. of Chemical and Biochemical Engineering, Irvine, CA 92697-2575

ABSTRACT

The state of the art (SOA) Li-ion cells utilize carbon anodes. However, to improve specific energy, energy density, and safety of cells using carbon anodes, alternative anodes must be developed. Recently, Fuji Film Inc. has suggested the use of tin oxide based anodes in Li-ion cells. It is believed that cells containing tin oxide based anodes have the potential to meet the need for NASA's future missions. As a result, we conducted an analysis to compare the performance of cells containing carbon anodes and cells containing tin oxide anodes. The comparison between these cells involved the following: 1) reaction mechanisms between Li and carbon and reaction mechanisms between Li and tin oxide, 2) half cell and full cell performance characteristics, 3) interactions between the anode materials and electrolyte types and compositions, and 4) the optimization of binder composition.

INTRODUCTION

JPL is involved in the development of rechargeable lithium cells for future Mars Exploration Missions. Mars Exploration Missions can be broadly classified into four types: orbiters, landers, rovers and penetrators. These missions have some common performance requirements, such as high specific energy and energy density due to mass and volume limitations. However, each of these missions has some unique primary performance drivers, such as, long cycle capability (orbiters) and ability to operate at low temperatures (landers, rovers and penetrators). The orbiters require a cycle life greater than 30,000 cycles at 20-30% depth of discharge with a specific energy > 100 Wh/kg. The landers and rovers require batteries that can provide > 120 Wh/kg and operate at temperatures < -20 °C, whereas, the cycle life requirement is < 500 cycles (50-70% DOD). Penetrators require batteries that can operate at temperatures lower than -60 °C and withstand high shock levels. The lithium-ion system was selected for near term missions as this technology was more mature compared to the lithium metal based and lithium polymer battery systems. The specific objectives of the JPL lithium ion cell effort are: 1) Improve the low temperature performance of lithium-ion cells and demonstrate their applicability to lander, rover and penetrate missions, 2) Improve the cycle life performance of lithium-ion cells and demonstrate the ability to meet life requirements of the Mars orbiters and 3) Establish effective charge methodology and reconditioning methods for on-board battery management. To realize these objectives work is in progress in areas such as chemistry and material development, design optimization and data base development. The prime objective of the chemistry and materials subtask is to develop/select electrode materials and electrolytes that are capable of providing long cycle life and improved low temperature performance.

The SOA Ni-Cd and Ni-H₂ batteries are quite heavy and bulky and cannot meet mass and volume requirements of future Mars missions. Furthermore, they have very poor low temperature performance capability as they use aqueous electrolytes. Rechargeable lithium-ion batteries offer significant weight, volume and cost advantages compared to SOA Ni-Cd and Ni-H₂ batteries and are especially attractive for future Mars Missions. The performance advantages include: higher specific energy (2 to 3 times greater than Ni-Cd and Ni-H₂), energy density (3-4 times greater than Ni-Cd and Ni-H₂), higher cell voltage, coulombic and energy efficiency, low self-discharge rate, and lower battery costs compared to the SOA Ni-Cd and Ni-H₂ batteries. These advantages translate into several benefits for Mars Missions including: reduced weight and volume of the energy storage subsystem, improved reliability, extended mission life, and lower power system life cycle costs.

Four types of lithium cells are presently under development in the US, Europe and Japan: 1) lithium metal with liquid electrolyte, 2) lithium metal with polymer electrolyte 3) lithium-ion containing liquid electrolyte, and 4) lithium-ion containing polymer electrolyte. Among these four types of technologies, lithium-ion battery technology is the most advanced and likely candidate for future space missions (1998 and beyond). This system is also being considered by other aerospace organizations for GEO and LEO spacecraft applications. These cells employ a carbon/graphite anode (instead of metallic lithium) and liquid organic electrolytes. LiCoO_2 , LiNiO_2 , and LiMn_2O_4 are presently being evaluated by several commercial vendors as candidate cathode materials for these cells. Small capacity cylindrical cells have been introduced into the United States by Japanese manufacturers for portable electronic applications. These cells have a specific energy of about 80-120 Wh/kg and 200-240 Wh/l and can operate at temperatures in the range of -10 to 30°C. These cells can deliver >500 deep discharge cycles. For future Mars exploitation applications, however, certain improvements must be made in order to meet specific mission requirements, such as improving the cycle life of the cells, extending the operating range to lower temperatures, as well as scaling-up the technology to large cell sizes (5-20 Ah).

At present, carbon materials, such as coke and graphite, are used as anode materials in rechargeable lithium-ion cells. These materials exhibit lower usable specific capacity (150-300 mAh/g) compared to metallic lithium and this results in lower specific energy. Additionally, carbon-based anodes typically have low densities, which imposes limits on the energy density of the Li-ion batteries. Moreover, carbon anodes operate at potentials very close to that of lithium and, consequently, are reactive and may exhibit safety problems especially in large size batteries.

In order to further improve the specific energy, energy density, and safety of lithium-ion cells, advanced anode materials alternative to carbon anodes with higher specific capacity and stability need to be developed. Of the alternative rim-carbon anode materials, lithium alloys appear to be attractive. Lithium alloys usually have high specific capacity of lithium. The major problem which limits their use is the volumetric instability of the lithium alloy electrode during charge and discharge cycling. However, recent developments suggest that lithium alloys may work well as anode materials for Li-ion cells. Fujifilm Inc. in Japan has announced a successful development of a Li-ion cells containing amorphous tin-based composite oxide anodes⁽¹⁾. It has been suggested that the reaction of lithium and tin oxide will form tin metal and lithium oxide initially⁽²⁾, the continuation of lithium insertion after the lithium oxide formation leads to the reaction between lithium and tin metal.

At JPL, a preliminary analysis was conducted to compare and evaluate carbon and tin oxide anodes for use in Li-ion cells⁽³⁾. It is the purpose of this paper to report the results of this comparison which includes the following: i) the mechanisms that occur when Li reacts with both carbon and tin oxide, ii) cycling performance of carbon vs. tin oxide, iii) the effects of electrolyte types and compositions in cells containing carbon and tin oxide anodes, and iv) the optimization of binder composition of tin oxide anodes.

EXPERIMENTAL

The electrochemical evaluation of carbon, SnO, and SnO₂ anodes was conducted using half-cells with the electrodes wound in a spiral configuration. In the half-cell configuration, lithium was used as the anode and reference electrode, and carbon, SnO, and SnO₂ electrodes were used as the cathode. The carbon, SnO and SnO₂ electrodes were made by spraying a solution containing either carbon, SnO, or SnO₂ powder, Poly(vinylidene fluoride) (PVDF) binder, and carbon black onto a copper foil substrate. Lithium electrodes were made by cold pressing lithium foil onto nickel mesh substrates. In the full-cell configuration, LiCoO₂ was used as cathode material, carbon or tin oxides were used as anodes. The anodes and cathodes were separated by two layers of 1 mil thick polypropylene membranes. The cells were activated with the various mixed solvent electrolytes containing LiPF₆ salt dissolved in Ethylene Carbonate (EC), Dimethyl Carbonate (DMC), Diethyl Carbonate (DEC), Butylene Carbonate (BC) and Propylene Carbonate (PC). All cell assembly operations were carried out in an oxygen and moisture free glove box. The experimental cells were evaluated for charge/discharge characteristics, faradaic utilization of the active material, rate capability and cycle life. Constant current was used for charging and discharging the cells, Open circuit voltages (OCV) were determined using a coulometric titration technique.

Preparation of high specific surface area crystalline SnO was achieved by using a modified precipitation technique, as follows: 1) dissolving SnCl₂·2H₂O (Alfa 99.99%) in distilled water, 2) the resulting solution was added dropwise into a 1 N NaOH solution (Fisher Scientific), 3) additional NaOH was added to maintain a pH of 14 at all times, and lastly 4) a black aggregate formed which was then washed with distilled water, filtered, and allowed to dry in air at room temperature. The commercial tin oxides were obtained from (Alfa 99.99%). X-Ray Diffraction (XRD) was used to identify crystalline phases, and determine average grain sizes, for in-house prepared SnO and commercially obtained SnO powder. A standard B.E.T. analysis determined the average specific surface areas for both SnO powders. The average particle sizes of the SnO powders were determined using a laser light scattering technique. Surface morphologies for both powders were examined using Scanning Electron Microscopy (SEM).

To determine the crystalline phases present after lithium was titrated into the SnO and SnO₂ powder the following procedure was used: 1) 5 SnO half cells and 5 SnO₂ half cells were made using the procedure mentioned above, 2) the amount of lithium titrated into each SnO or SnO₂ electrode was pre-determined, 3) after titrating lithium into each electrode the open circuit voltages (OCV) were measured, 4) the cells were then opened in a glove box and the electrodes were washed in solvent and sealed in a polypropylene bag, 5) the electrodes were then analyzed using XRD to determine the crystalline phases present.

RESULTS AND DISCUSSIONS

(1) Comparison of reaction mechanism:

Graphite and Coke

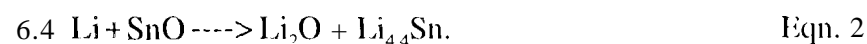
The graphite structure consists of layers of carbon atoms arranged in hexagonal rings that are stacked in an ABAB . . . sequence. In coke, the basic structural unit is similar to graphite, however, its carbon layers have small lateral sizes and the stacking of the layers is imperfect and characterized by a turbostratic structure. The reaction mechanism between Li and graphite is an intercalation type reaction and proceeds in stages as follows: C --> LiC₂₄ --> LiC₁₈ --> LiC₁₂ --> LiC₆, where the formation of each of these LiC_x phases corresponds to the constant voltage plateaus in the charge/discharge curve in the Li/C system. It is important to note that during this reaction, there are no major structural reconfigurations in graphite, which results in a highly reversible reaction. However, when graphite is initially charged, the formation of a passivation layer due to electrolyte decomposition at the electrode surface is immanent, and results in an irreversible capacity loss. Additionally, the average discharge voltage for the intercalation of Li into graphite is approximately 0.1 V, which will be compared to the Li-tin oxide system, shortly. Unlike graphite, the reaction mechanism between Li and coke is a solid solution reaction and therefore the charge/discharge curves for coke have no voltage plateaus but instead have sloped curves between 1.0 and 0 volts. In Li-ion cells containing carbon anodes, graphite anodes are preferred to coke due to the higher reversible capacity of graphite. However, when compared to graphite, coke has higher rate capabilities which results from the open structure, of coke. Additionally, compared to graphite, coke has a higher lithium potential gradient.

Crystalline SnO and SnO₂

SnO₂: The reaction that occurs when Li is titrated into tin oxide is not an intercalation reaction, instead it has been suggested that a constitutional metal ion occurs according to the following equation for SnO₂ (rutile):



Hence, the reaction that occurs for SnO (layered type structure) is:



In Figure 1 the charge/discharge curves are shown for Li/SnO and Li/SnO₂. From Figure 1, it is observed that 8.15 moles of Li reacted with SnO₂, which is in agreement with the 8.4 moles predicted from equation 1. From equation 1, out of the 8.4 moles of Li initially titrated into SnO₂, 4 moles of Li are irreversibly consumed to form 2 moles of Li₂O, and 4.4 moles of Li are reversibly stored in 1 mole of Li_{4.4}Sn. However, it is observed that only 2.9 moles of Li were extracted during charging, which is not in agreement with the 4.4 moles of Li predicted by equation 1. It is believed that the decrease in the reversible capacity can be attributed to the fact that 2 moles of Li₂O are formed for every mole of SnO₂ compared to only 1 mole of Li₂O formed for every mole of SnO. Although Li₂O is a reasonably good Li-ion conductor, its conductivity is still considerably less than that of the liquid organic electrolyte. Therefore, it is believed that the increase in Li₂O formation for SnO₂ significantly increases polarization effects. By doing this, the resulting conditions are far from equilibrium. The net result is a decrease in the reversible Li capacity for SnO₂ for a fixed current density.

The data of Figure 1 suggests that the plateau from 0 to approximately 3 moles of Li, represents the decomposition of SnO₂ into Li₂O and Sn as indicated by the corresponding line segment spanning from x = 0 to x = 4.0 moles of Li in the proposed Li-Sn-O ternary phase diagram (Figure 2). (The ternary phase diagram is used as a "thinking tool" to assist in the understanding of the Li-Sn-O system) However, equation 1 and the phase diagram shown in Figure 2 predict that this reaction should consume 4.0 moles of Li. It is believed that this difference is due to the fact that the voltage values indicated along the discharge/charge curve do not represent OCV (equilibrium voltages), because they are measured under an applied current. According to the OCV measurements listed in Table I, it is observed that the OCV for 1.5, 2.5, and 4.0 moles of Li titrated into 1 mole of SnO₂ are 1.16 V, 1.10 V and 1.09 V, respectively. However, when more than 4.0 moles of Li are titrated into SnO₂, the voltage drops significantly to 0.76 V for 5.5 moles of Li. From this, it is apparent that the amount of Li consumed during the first plateau is approximately 4.0 moles as indicated by the significant decrease in the OCV after x = 4.0 as predicted by Figure 2. Altogether, by measuring the OCV for the cells listed in Table I, rather than estimating the length of the plateau using the discharge/charge curve (Figure 1), a more accurate value for the amount of Li consumed to irreversibly form Li₂O can be determined. Thus, the experimentally determined value of 4.0 moles of Li consumed to form 2.0 moles of Li₂O is in agreement with the predicted value.

Table I. OCV Measured for the SnO₂ Half Cells

Moles of Li	OCV vs. Li (Volts)
1.5	1.16
2.5	1.10
4.0	1.09
5.5	0.76

In Figure 3 the XRD patterns are shown for the cells listed in Table I. In Figure 3, when Li is titrated into SnO₂ (from x = 1.5 to x = 8.0) the SnO₂ peaks are broadened and shortened when compared to the pure SnO₂ (x = 0). Additionally, Sn peaks are observed in the samples containing Li. From this, it can be concluded that the initial reaction of Li with SnO₂ results in the formation of Sn. The absence of any Li₂O peaks, which should be present from the predictions made by Figure 2, most likely suggests that the Li₂O is amorphous. According to Figure 2 when more than 4 moles of Li react with SnO₂ Li-Sn alloys should be present. However, the XRD patterns in Figure 3, do not indicate the presence of any Li-Sn alloys. It is suggested that the combined effects from the increased background noise that result from the presence of amorphous Li₂O and the fact that the Li-Sn peaks are relatively weak in intensity can explain the difficulties of identifying any Li-Sn peaks in the X-Ray diffraction patterns. However, to confirm this, further detailed work is required. Altogether, the confirmation that metallic Sn is formed from the reaction of Li with SnO₂, supports the validity of equation 1 and the phase diagram shown in Figure 2.

SnO: From Figure 1, it is observed that 6.25 moles of Li initially reacted with 1 mole of SnO, which is in good agreement with the 6.4 moles predicted by equation 2. Equation 2, predicts that out of the 6.4 moles of Li that react with SnO, 2 moles of Li are irreversibly consumed to form 1 mole of Li_2O , and 4.4 moles of Li are reversibly stored in 1 mole of $\text{Li}_{4.4}\text{Sn}$. From Figure 1, it is observed that 4.0 moles of Li are extracted from SnO, which is in close agreement with the 4.4 predicted by equation 2. The close agreement between the experimentally determined initial and reversible Li capacities with the theoretically determined capacities supports the validity of equation 2.

Table II. OCV Measured for the SnO Half Cells

Moles of Li	OCV vs. Li (Volts)
1.0	1.40
2.0	1.34
3.0	0.86
4.5	0.48
6.0	0.36

The data of Figure 1 shows that the length of the plateau, from 0 to approximately 2 moles of Li, represents the (decomposition of SnO into Li_2O and Sn as indicated by the line spanning from $x = 0$ to $x = 2.0$) moles of Li shown in Figure 4. To obtain the true equilibrium voltages as a function of the moles of Li, the OCV were again measured and listed in Table 11, from this it is observed that the OCV for 1.0 and 2.0 moles of Li reacted with 1 mole of SnO are similar (1.40 and 1.34 V, respectively). However, when more than 2.0 moles of Li react with SnO, the voltage drops significantly to 0.86 V for 3.0 moles of Li and eventually to 0.36 V for 6.0 moles of Li. The relatively constant OCV measured from 1.0 to 2.0 moles of Li further confirms that the length of the initial plateau in Figure 1 between 0 and 2.0 moles of Li. The similarities between the predicted amount of 2.0 moles of Li consumed to form 1 mole of Li_2O and the amount of Li consumed during the initial plateau in Figure 1, (approximately 2 moles Li), further supports the validity of equation 2.

In Figure 5 the XRD patterns are shown for the SnO half-cells listed in Table 11. The phase diagram in Figure 4 predicts that: i) the amount of SnO should decrease from $x = 0$ to $x = 2.0$ moles of Li, and ii) at $x = 2.0$ moles of Li, SnO should not be present. Likewise, according to XRD patterns for $x = 0$ to $x = 2.0$ moles of Li, the heights of the SnO diffraction peaks and therefore the amounts of SnO decrease. At $x = 2.0$ moles of Li, the absence of SnO peak confirms the absence of SnO. Furthermore, the phase diagram in Figure 4 predicts that the maximum amount of Sn present occurs at $x = 2.0$ moles of Li. Correspondingly, according to the XRD pattern for $x = 2.0$ moles Li, the height of the Sn peak and therefore the amount of Sn is at a maximum when compared to all of the other samples. It is important to note that since the XRD peak heights change as a function of the amount of a particular phase present, the amount of material analyzed has a significant effect on the peak height. However, all of the SnO samples listed in Table II were carefully weighed to assure that the amounts of SnO analyzed were all the same. Altogether, the strong agreement between the predictions made by Figure 4 and the XRD patterns shown in Figures 5 further confirms the validity of Equation 2.

Amorphous (Fine-Grained) SnO₂

In Figure 6, the discharge/charge curves are shown for both the amorphous SnO₂ (SnO₂-AM) and crystalline SnO₂ (SnO₂-C). In Figure 7, the XRD patterns are shown for both the SnO₂-AM and SnO₂-C samples after Li titration (10.20 moles of Li into SnO₂-AM and 8.15 moles of Li into SnO₂-C). From Figure 6 it is observed that 10.20 moles of Li were titrated into SnO₂-AM and 8.15 moles of Li were titrated into SnO₂-C. The plateau region for the SnO₂-C from $x = 0$ to $x = 4.0$ moles of Li during discharging, represents the transformation of SnO₂ into Li_2O and Sn (discussed in detail above). Conversely, no plateaus are observed for the SnO₂-AM sample thus, it is believed that the SnO₂-AM does not undergo significant phase changes. Instead, it is believed that when Li reacts with SnO₂-AM, Li_xSnO_2 is formed, as confirmed by the absence of well defined crystalline peaks in the XRD patterns.

From Figure 7 it is observed that the SnO₂-AM remained relatively amorphous with the exception of the short broad Sn peaks which “indicate the presence of Sn. However, it is important to note that the SnO₂-AM is not truly amorphous, instead it is only considered fine-grained. Therefore, it is believed that the fine SnO₂-AM grains undergo the same reaction as the SnO₂-C, since they are both crystalline. But, since the SnO₂-AM is fine-grained, a majority of the SnO₂-AM exists in the amorphous condition. As a result, the amount of Sn present in the SnO₂-AM, after Li titration, is proportional to the amount of crystalline SnO₂ present, before Li titration. Consequently, since the amount of crystalline SnO₂ present in SnO₂-AM is relatively low, the amount of Sn formed is correspondingly low. Altogether, since the SnO₂-AM does not undergo a phase change, with the exception of its crystalline components, it can be considered an insertion anode. Whereas SnO₂-C undergoes a decomposition, which results in the formation of Li₂O and Sn, and it is the Sn which acts as the active anode material.

From Figure 6, it is also apparent that the reversible Li capacities for both SnO₂-AM and SnO₂-C are 2.90 and 3.00 moles of Li, respectively. The fact that these capacities are similar cannot be explained since it is suggested that the SnO₂-AM electrode remains amorphous Li_xSnO₂, and SnO₂-C forms a Sn/Li₂O microstructure.

(2) Performance comparison (Coke, Graphite, and tin oxide):

Anode Specific Capacity

Typically, the performance of anode materials is compared by their specific capacity in mAh/g. The specific capacities for Graphite, Coke, SnO and SnO₂ are listed in Table 111. From Table 111, it is “observed” that SnO has the highest reversible capacity, while coke has the lowest. Additionally, SnO₂ has the highest irreversible capacity, while graphite has the lowest.

Table 111. Comparison of reversible and irreversible capacities

Anode	Irrev.Cap. mAh/g	Rev. Cap mAh/g	Irrev/Rev Ratio
Graphite	42	272	0.15
Coke	85	173	0.49
SnO	444	793	0.56
SnO ₂	936	501	1.87

Predicted Cell Specific Energy and Energy Density

The densities of SnO and SnO₂ are 6.5 g/cm³ and 6.99 g/cm³, respectively. Therefore, a Li-ion cell containing a tin oxide anode, 1 LiCoO₂ cathode, will have a predicted specific energy greater than 140 Wh/Kg, and a energy density of 300 Wh/l. in comparison, the average density of carbon is 2 g/cm³ and therefore, a Li-ion cell containing a carbon anode will have a lower specific energy and energy density compared to tin oxide (100 Wh/Kg, and 240 Wh/l, respectively).

Discharge Characteristics of Full and Half Cells

The discharge profiles for Li-ion cells containing graphite, coke, and tin oxide anodes, and LiCoO₂ cathodes are different. The discharge curves for graphite, coke, and tin oxide are shown in Figure 8. It is observed from Figure 8, that the discharge curve for graphite is relatively flat, whereas the coke and tin oxide discharge curves are sloping. The corresponding anode potential vs. Li and the cell operating voltages are listed in Table IV.

Table IV. Comparison of half/full cell average voltages

Anode	Voltage vs. Li (Volts)	Cell Voltage (V)
Graphite	0.1	3.8
Coke	0.3	3.6
Tin Oxide	0.5	3.4

Effects of Particle Size

Typically, high specific surface area carbon powders are desired to maximize the accessible reaction area. This in turn, results increased cell rate capabilities. However, for Li-ion applications, by increasing the carbon specific surface area the relative amount of passivation film formed is correspondingly increased. Therefore, there is an optimal specific surface area (5-10 m²/g) to which a balance can be established between cell rate capability and irreversible Li capacity loss.

Unlike carbon powders, the irreversible capacity loss in tin oxide is not attributed to surface reactions with the electrolyte. Instead, the irreversible loss is considered to be due to a bulk reaction and is therefore not dependent of specific surface area. As a result, high specific surface area tin oxide powders are preferred to enhance cell rate capabilities.

3) Electrolyte Analysis

An analysis was conducted to determine the effect of electrolyte types and compositions on cycle life. Different compositions of electrolyte containing LiPF₆ salt dissolved in Ethylene Carbonate (EC), Dimethyl Carbonate (DMC), Diethyl Carbonate (DEC), Butylene Carbonate (BC) and Propylene Carbonate (PC) were used in half cell. All cells were tested using a discharge current density of 0.344 (mA/cm²), and a charge density of 0.172 (mA/cm²). In this analysis the following effects were investigated: a) the effect of varying the electrolyte compositions on the irreversible/reversible capacities, b) the effect of electrolyte types on cycling performance, and c) the effects of EC composition on cycling performance.

a) The irreversible, reversible, and the reversible/irreversible Li capacity ratios for the initial cycle in cells containing different EC/DMC electrolyte compositions are shown in Table V. From Table V, it is observed that the 10EC/90DMC electrolyte yields the highest irreversible and reversible capacities whereas the 50EC/50DMC electrolyte yields the lowest irreversible and reversible capacities. It is important to note, however, that the reversible/irreversible capacity ratios for the 10EC/90DMC, 30EC/70DMC, and 50EC/50DMC electrolytes are the same. It is believed that the increase in the amount of EC increases electrolyte viscosity thus, resulting in increased polarization effects. As a result, the irreversible and reversible capacities change proportionally by varying the amount of EC present in the electrolyte.

On the contrary, the irreversible and reversible Li capacities do not change proportionally for carbon anodes. For example, in cells containing carbon anodes with EC/DMC electrolyte, by increasing the amount of EC the reversible capacity remains the same whereas the irreversible capacity increases (Fig. 9). The fact that the reversible capacity for carbon is relatively insensitive to the amount of EC indicates that polarization effects are minimal. Therefore, since it is known that EC decomposes readily on the carbon surface to form a passivating layer, it is suggested that by increasing the amount of EC a proportional increase in the amount of decomposition product on the carbon surface results. Hence, the irreversible Li capacity increases as the amount of EC increases.

Table V. Effects of EC/DMC composition on irreversible and reversible capacities

EC/DMC Compositions	irreversible. Cap. (mole Li/mole SnO)	Reversible Cap. (mole Li /mole SnO)	Rev./Irrev
10/90	2.330	2.408	1.033
30/70	2.059	2.232	1.084
50/50	2.001	2.101	1.050

It was determined that the irreversible Li capacity of tin oxide to be insensitive, to the electrolyte composition but is highly dependent on the electrolyte type.

b) The reversible Li capacity vs. cycle number plot is shown in Fig. 10 for three SnO half cells containing: i) 30EC/70DMC, ii) 30BC/70DMC, and iii) 50PC/50DEC. From Fig. 10, it is observed that the capacity decline is most severe for the cell containing 50PC/50DEC electrolyte, whereas the cell containing 30EC/70DMC yielded the highest cycle life performance. The reasons for this are not clear at the moment.

c) The reversible Li capacity vs. cycle number plot is shown in Fig. 11 for three SnO half cells containing: i) 30BC/70DMC, ii) 10EC/30BC/60DMC, and iii) 40EC/10BC/50DMC. From Fig. 11 a trend is observed which indicates that as the amount of EC increases the cycle life performance improves. Since EC alone is viscous (solid at room temperature) it is believed that by increasing the amount of EC, the viscosity of the electrolyte increases, which in turn acts to reinforce the $\text{Li}_2\text{O}/\text{Sn}$ composite electrode during cycling.

4) Binder Composition Analysis

An analysis was conducted to determine the optimum PVDF binder composition in carbon and SnO electrodes. It is known that the amount of binder affects the electrode performance. In the case of carbon electrodes, the amount of binder affects the reversible and irreversible Li capacity. The voltage vs. Li capacity is shown in Fig. 12 for three SnO half cells containing 10 % carbon black and: i) 5.5% binder, ii) 11% binder, and iii) 15.4% binder. From Fig. 12 several observations can be made. Firstly, it is observed that the initial capacity increases with decreasing amounts of binder. Secondly, the electrodes containing 5.5 and 11% binder have the same reversible capacity whereas the electrode containing 15.4% binder has a significantly lower reversible capacity.

The Li capacity vs. cycle number plot is shown in Figure 13. From Figure 13, it is apparent that up to 7 cycles the electrode containing 5.5% binder has the highest capacity, while the electrode containing 15.4% binder has the lowest. However, after 7 cycles, the capacity of the electrode containing 5.5 % drops below that of the electrode containing 11% binder. This suggests that 5.5% binder is not sufficient to counteract the effects of severe volume changes that occurs during cycling. Therefore, to optimize cycle life performance it is suggested that the binder composition is 11%.

SUMMARY

In this study, it was determined that half and full cells containing carbon and tin oxide anodes have significantly different behavior. Firstly, the initial reaction between Li and tin oxide results in the decomposition of tin oxide into metallic Sn and Li_2O . Upon further addition of Li, Li reacts with Sn to form several Li-Sn alloys. Therefore, the reaction of Li with tin oxide is considered to be a reconstitutive reaction whereas the insertion of Li into carbonaceous materials is an intercalation type reaction for graphite and a solid solution type reaction for coke. Secondly, the discharge profiles for cells containing graphite have a relatively constant voltage during cycling whereas the voltage of cells containing tin oxide and coke anodes decreases continuously. Additionally, it was determined that the capacity fade rate for cells containing coke anodes is the lowest. The capacity fade rate for graphite decreases steadily, but is considerably lower than that of tin oxide. Thirdly, the irreversible Li capacity of cells containing tin oxide anodes was found to be insensitive to electrolyte composition but is highly dependent on electrolyte type. In addition, it is believed that by increasing the amount of EC, the viscosity of the electrolyte increases, which in turn acts to reinforce the $\text{Li}_2\text{O}/\text{Sn}$ composite electrode during cycling. Furthermore, for Li-ion cells containing carbon anodes, the irreversible capacity during the first cycle is due to electrolyte decomposition, which results in irreversible film formation on the carbon surface. This irreversible capacity is highly dependent on the electrolyte type and composition. In this study, electrolytes containing higher percentages of EC showed higher initial irreversible capacities. Hence, a tradeoff in the electrolyte composition may be necessary to obtain optimal rate capability and cycle life while minimizing initial irreversible loss. Lastly, it was determined that the optimum binder composition which yields the lowest capacity fade rate for SnO is 11% PVDF.

ACKNOWLEDGMENT'S

The work described here was carried out at Jet Propulsion Laboratory, California institute of Technology, under contract with the National Aeronautics and Space Administration.

References

1. Yoshio Idota, etc., European Patent # 065 1450A1.
2. 1. A. Courtney, A. M. Wilson, W. Xing and J. R. Dahn, Paper presented in the Electrochemical Society Fall Meeting held at San Antonio, Texas, Oct. 6-11, 1996.
3. J. S. Sakamoto, Master's thesis, University of California, Irvine (1997).

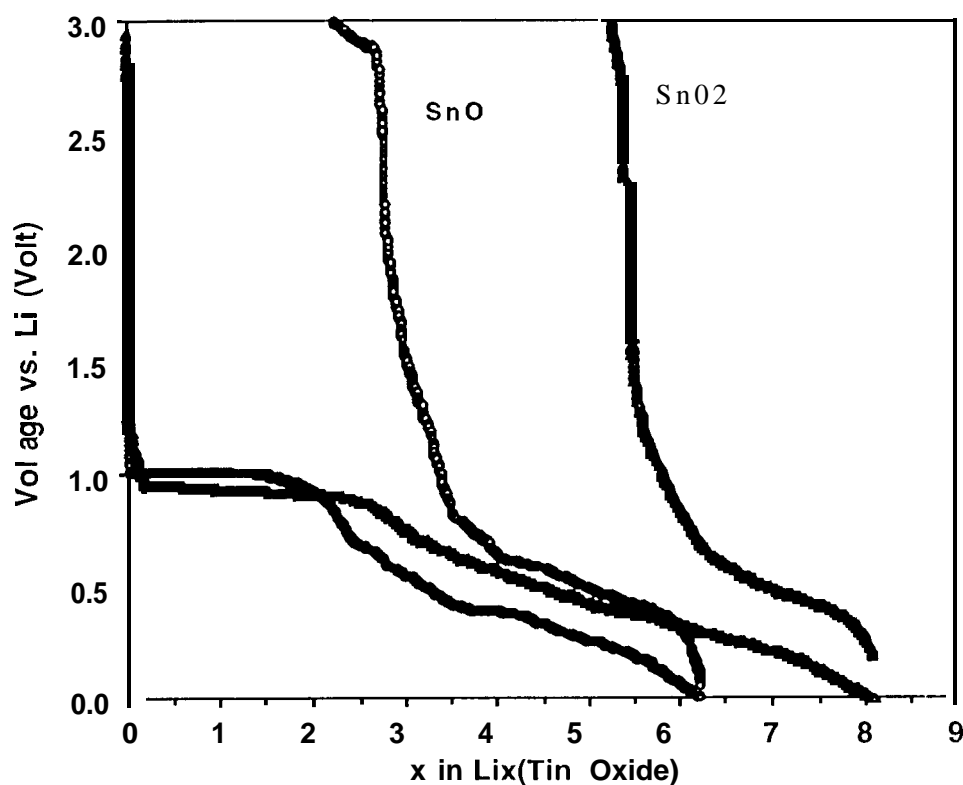


Figure 1. Discharge/charge curves for SnO₂ and SnO.

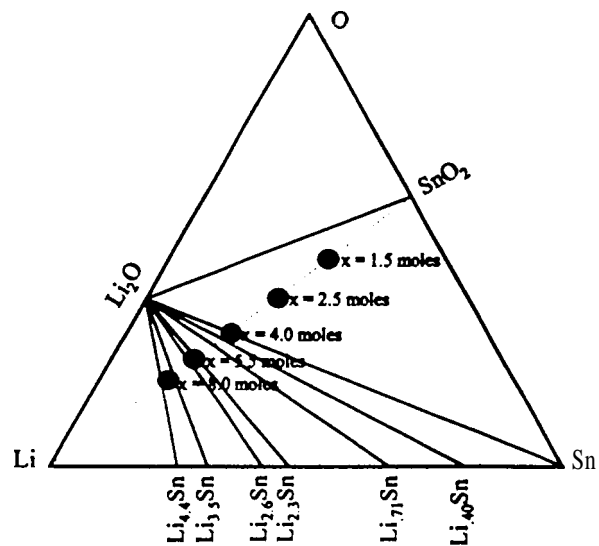


Figure 2. SnO₂ cell compositions plotted on Li-Sn-O phase diagram (x = moles of Li)

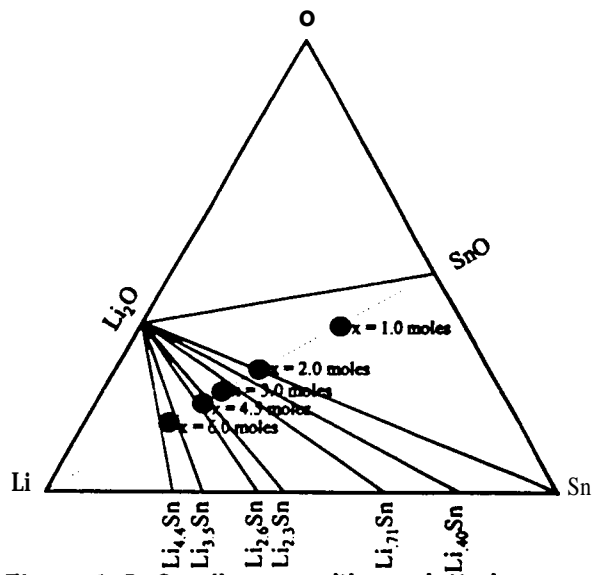


Figure 4. SnO cell compositions plotted on Li-Sn-O phase diagram (x = moles of Li)

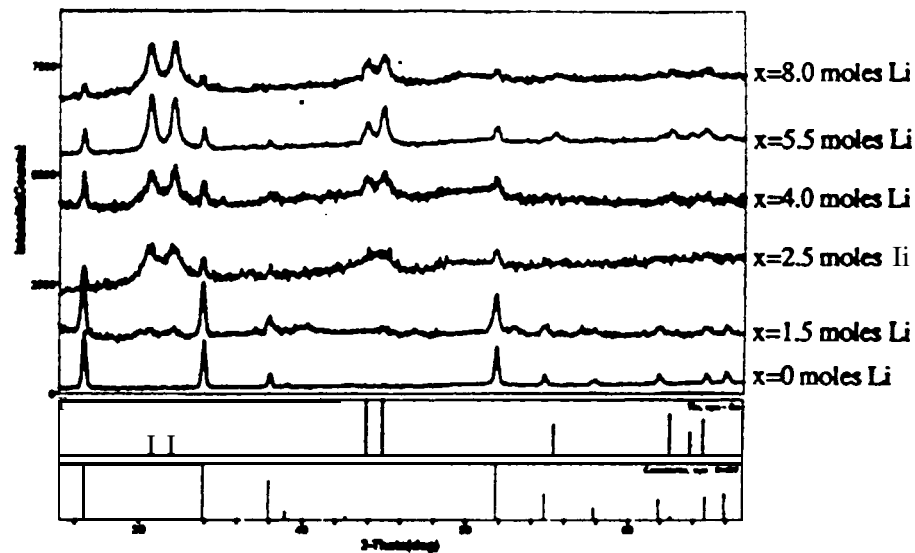


Figure 3. XRD patterns for Li/SnO₂ half cells

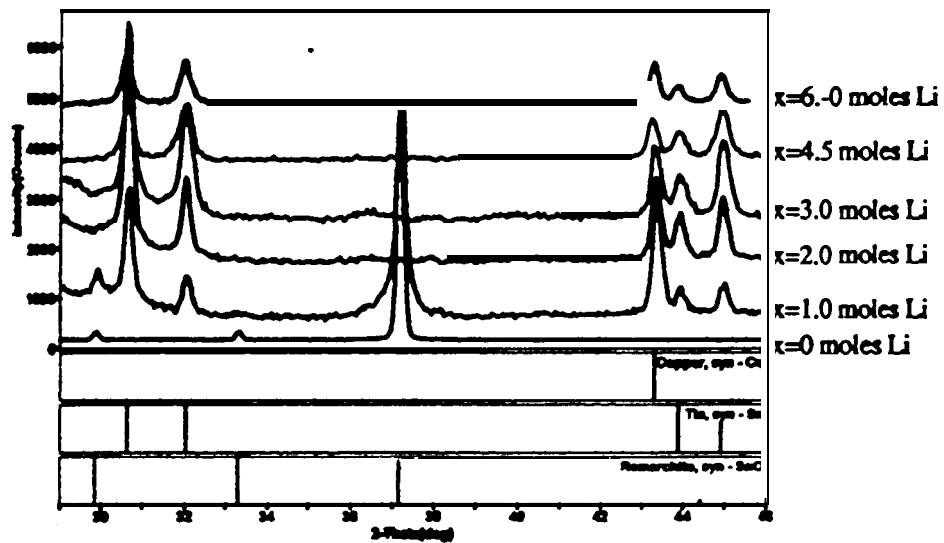


Figure 5. XRD patterns for SnO half cells

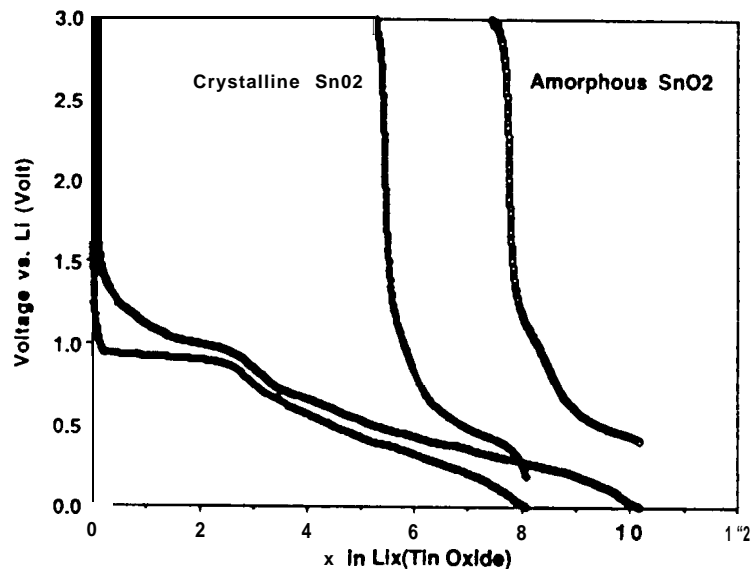


Figure 96. Discharge/charge curves for SnO₂-AM & SnO₂-C

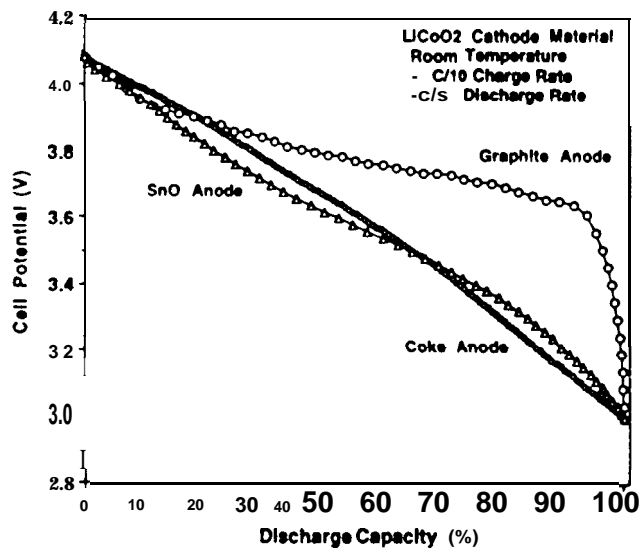


Figure 8. Discharge characteristics of Li-ion cells containing various anode materials

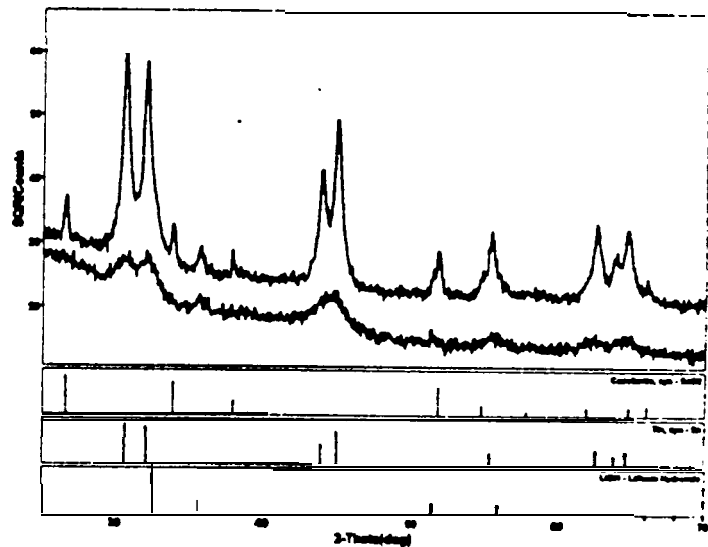


Figure 7. XRD patterns for SnO₂-AM after Li was titrated in (a), and SnO₂-C after Li was titrated in (b)

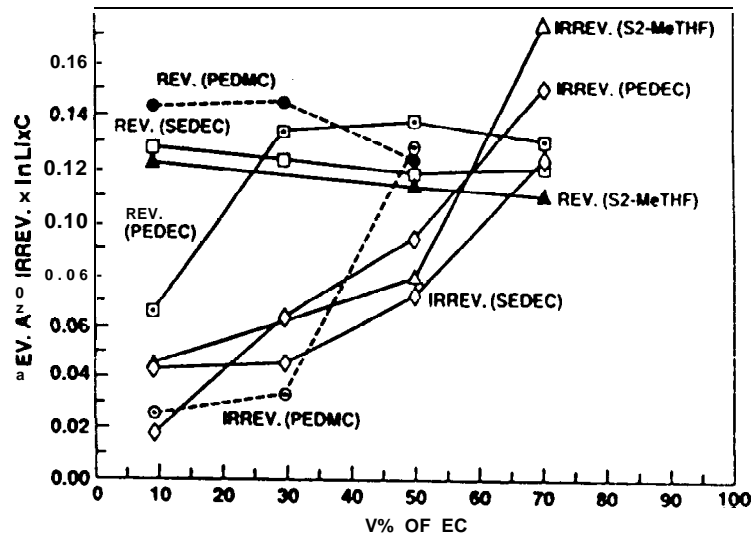


Figure 9. Comparison of the reversible and irreversible capacities in LVC cells with various electrolytes

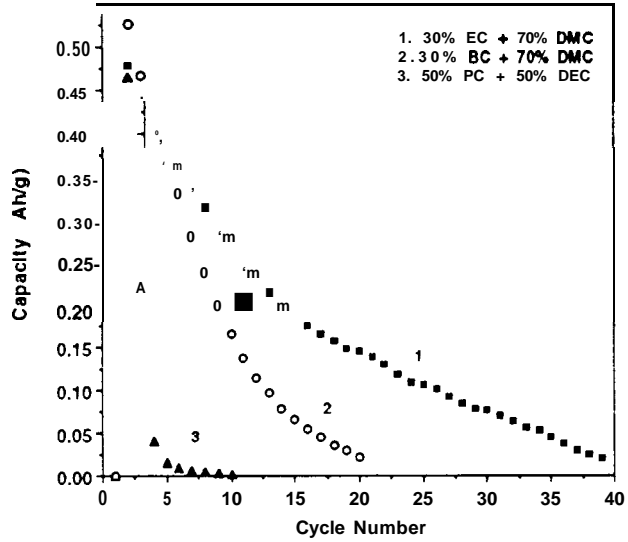


Figure 10. Effect of electrolyte type on cell cycling performance

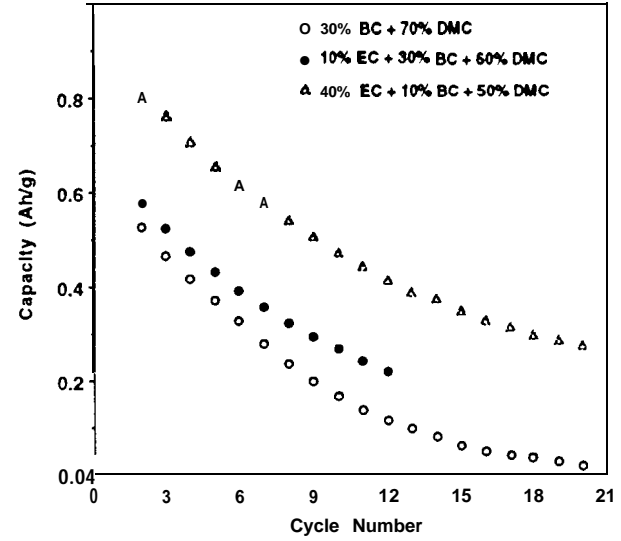


Figure 11. Effect of EC percentage on cell cycling performance

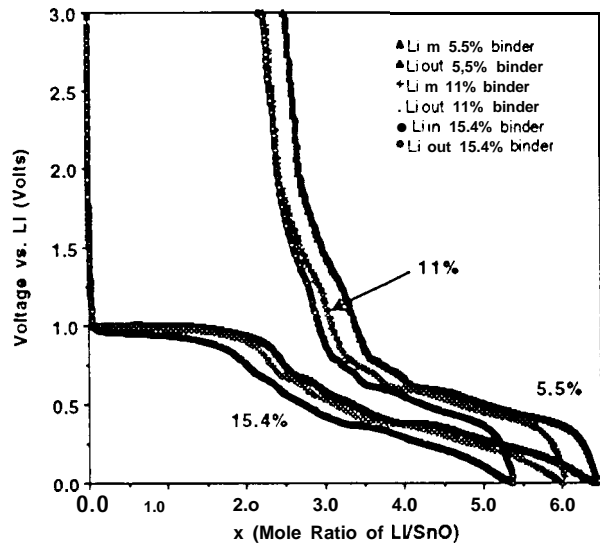


Figure 12. Effect of binder composition on initial cycle

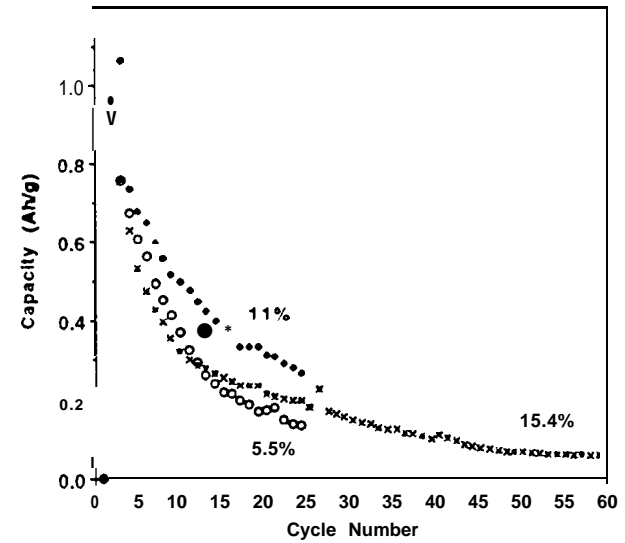


Figure 13. Comparison of cycling performance of SnO electrodes with various binder amounts